

Motion of a colloidal particle in a nonuniform director field of a nematic liquid crystalBeom-Kyu Lee,¹ Sung-Jo Kim,^{1,*} Bohdan Lev,^{1,2} and Jong-Hyun Kim^{1,†}¹*Department of Physics, Chungnam National University, 99 Daehak-ro, Yuseong-gu, Daejeon 34134, Korea*²*Bogolyubov Institute for Theoretical Physics of the NAS of Ukraine, Metrolohichna Street 14-b, Kiev 03680, Ukraine*

(Received 1 December 2016; published 27 January 2017)

We investigate the dynamics of a single spherical particle immersed in a nematic liquid crystal. A nonuniform director field is imposed on the substrate by a stripe alignment pattern with splay deformation. The particle of homeotropic anchoring at the surface is accompanied by hyperbolic hedgehog or Saturn-ring defects. The particle motion is dependent on the defect structure. We study the two types of motions theoretically and confirm the obtained results experimentally. The particle accompanied by a hyperbolic hedgehog defect is pulled to a deformed region to relax the elastic deformation energy. The motion occurs in the direction heading the hyperbolic hedgehog defect of a particle in a twist region. The position exhibits a weak S-shaped change as a function of time. The particle accompanied by a Saturn-ring defect shows insignificant motion due to its relatively small deformation energy.

DOI: [10.1103/PhysRevE.95.012709](https://doi.org/10.1103/PhysRevE.95.012709)**I. INTRODUCTION**

Nematic colloidal systems consist of a nematic liquid crystal (NLC) host and colloidal particles. Such systems show diverse behaviors depending on their physical properties. NLCs tend to reduce the director deformation and prefer a uniform arrangement [1]. The colloidal particles embedded in an NLC host cause a deformation of the director orientation. The tendency of an NLC to reduce the deformation gives rise to various colloidal particle structures, which are strongly dependent on particle characteristics such as surface anchoring conditions, shape, and size. In addition, these structures are susceptible to flow, external electric or magnetic fields, etc.

Colloidal particles in NLCs are accompanied by defects around them, with the defect structure and director distribution determined by the surface anchoring conditions of these particles. The boojum defect is created when the director aligns tangentially on the particle surface [2,3], whereas the Saturn-ring or hyperbolic hedgehog defects arise when the director aligns vertically on the particle surface [4,5]. The director field near the particle is responsible for interparticle interactions [6–8].

The director field and defect structure around a single particle can be changed by external electric or magnetic fields. When an external field was applied parallel to the far-field director direction, particles with homeotropic anchoring induced a transformation of a Saturn-ring defect into a hyperbolic hedgehog defect, which was experimentally identified and numerically analyzed [9,10]. The particle movement was induced by broken symmetry or controlled by changing the director using an external electric field [11,12].

The interparticle interactions in NLC hosts are also interesting. Two-particle interactions were measured dynamically in a homogeneous nematic cell with a Stokes drag force [4]. The theoretical investigations were performed using current, coat, and mirror image approaches [7,13–18], and numerical

modeling of these interactions was also developed [19–22]. These simulations showed that the above interactions are analogous to those of electric dipoles and quadrupoles. Even the motion of organizations such as bacteria was mediated by the elastic deformation [23,24]. The particle accompanied by a hyperbolic hedgehog defect acts as a dipole, and that with a Saturn-ring or boojum defect acts as a quadrupole. Therefore, these cases were termed the dipolar configuration (DC) and quadrupolar configuration (QC), respectively.

Typically, a nematic colloid is enclosed by two parallel flat substrates, with particle behavior being dependent on the boundary conditions at the particle and substrate surfaces. The interparticle interactions are dramatically changed by the electric field direction and confinement effects, as demonstrated experimentally and theoretically [14–20,22,25].

Interparticle interactions in nematic colloid systems are well documented. The motion of a single particle is expected to be governed by coupling with the distorted director region [7,13,20]. However, experimental investigations on the dynamics of a single particle coupled with the deformed director field are lacking. In this article, we used an NLC cell featuring a deformed director field with patterned alignment to observe the motions of DC and QC particles. The DC particle moved to the boundary of the alignment pattern, while the QC particle was motionless. This behavior is explained by the interaction between the particle and the deformed director field. The free energy of the DC particle was apparently dependent on its position inside the cell, making it move to the point of minimum energy. In contrast, the free energy of the QC particle seemed to be relatively independent of its position. Herein, detailed experimental and theoretical results are presented.

II. EXPERIMENT

Liquid crystal (LC) cells were fabricated by combining two glass substrates coated with different layers for planar alignment, with one substrate having an alignment pattern and the other one exhibiting uniform alignment. The patterned substrate possessed an orientation stripe pattern of repeating alignment orientation and 90°-rotated in-plane alignment

*Present address: IBS Center for Soft and Living Matter, UNIST-gil 50, Ulsan 689-798, Korea.

†jxk97@cnu.ac.kr

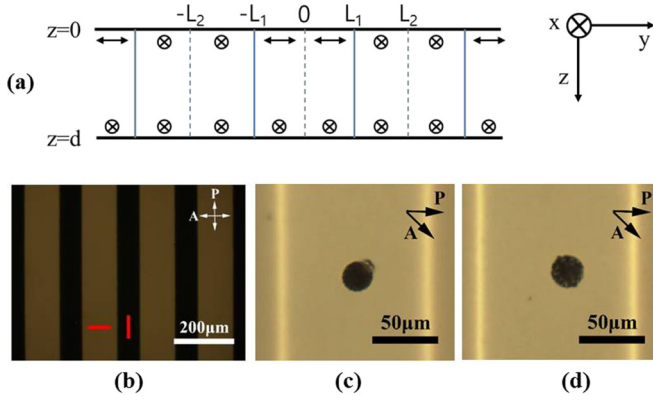


FIG. 1. (a) Schematic diagram of alignment in the LC cell. The upper substrate ($z = 0$) possesses an alignment pattern, which is alternately repeated in the x and y directions. The lower substrate exhibits uniform alignment (x direction). The pattern of the upper substrate is repeated every $2L_1$ and $2(L_2 - L_1)$ in the y direction. The LC director (\mathbf{n}) rotates in the x - y plane and is a function of y and z . The rotation angle $\phi(y, z)$ is defined as the angle with respect to the x axis. d is the cell gap. (b) Cell texture. The red line corresponds to the director direction on the surface of the upper substrate, $L_1 = 60 \mu\text{m}$, $L_2 = 100 \mu\text{m}$. The bright region exhibits a 90° twist alignment, while the dark region displays parallel alignment. The cell gap equals $70 \mu\text{m}$. (c) and (d) are images of the defects around particles acquired with the polarizer positioned in the y direction, and the analyzer positioned at 45° to the x direction. Both particles displayed in the images are located in the twisted region.

[Fig. 1(a)]. Thus, the LC in the cell can induce rotation only in the x - y plane by a certain azimuthal angle $\phi(y, z)$, which is a function of y and z . The substrate with an alignment pattern was prepared using photoalignment. The photoalignment material is a polyamic acid containing an azo unit in the main chain [26]. The azo unit undergoes *cis-trans* isomerization at light wavelengths around 400 nm. Normal irradiation on the substrate induces in-plane LC alignment, with the LC orientation being perpendicular to the polarization of light. The material was spin coated and softly baked. It was followed by irradiation with a focused diode laser light (405 nm) controlling the polarization and position. In fact, two alignment orientation regions characterized by a 90° difference in the azimuthal direction were produced. After the light irradiation, the substrate was baked at 200°C to stabilize the alignment. The other substrate was coated with a layer of polyimide (AL-3046) and rubbed for uniform planar alignment. The cell had a gap of $70 \mu\text{m}$.

Here, 4-cyano-4'-pentybiphenyl (5CB, Merck) was used as an LC matrix. It was of a nematic phase below 36°C and its density was 1.01 g/cm^3 [27]. The LC was injected at an isotropic phase to reduce the influence on alignment during injection. 5CB was mixed with polyethylene microparticles (GRYPMS, Cospheric) before the injection, being weakly homeotropically aligned at the particle surface [28,29]. The particle radii equaled $10 \pm 3 \mu\text{m}$, and their density equaled 1.0 g/cm^3 . Simplified LC parameters were used in the calculation. The one-constant approximation was adopted for the elastic constant. As the main interaction involved in the experiment was splay deformation, we used a splay elastic

constant of $3 \times 10^{-12} \text{ N}$ [30]. Even the actual shape of the particle accompanying a defect and the LC alignment were not isotropic, and the effective viscosities for any movement were considered to be the same, about $3.1 \times 10^{-3} \text{ N s/m}^2$ at 35°C [31].

Particle movement was observed through a polarizing optical microscope (Eclipse E600 from Nikon). We used a confocal microscope (TCS NT from Leica) to measure the vertical position of the particle in the cell. A dye, *N*, *N*-bis(2,5-di-tertbutylphenyl)-3,3,9,10-perylene-dicarboximide (BTBP, from Sigma Aldrich), was added in a small quantity. The temperature of the cell was maintained (TMS94 and LTS350 from Linkam) in the nematic phase of LC at 35°C , which is 1°C below the transition temperature.

III. RESULTS AND DISCUSSION

Figure 1(a) shows the cell structure and coordinate system used. The upper substrate possessed an alignment pattern, and the lower one exhibited uniform alignment. As both substrates featured planar alignment, the director changes could be described by the azimuthal angle variation in the x - y plane. The azimuthal angle ϕ was defined as the angle between the director orientation and the x axis. The director was invariant in the x direction, and its azimuthal angle was expressed as $\phi(y, z)$. The anchoring strength was assumed to be infinite on the alignment layer, with the director oriented along the alignment direction. Under these assumptions, the boundary conditions could be expressed as follows:

$$\phi(y, 0) = \begin{cases} \frac{\pi}{2}, & \text{for } -L_1 \leq y < L_1, \\ 0, & \text{for } -L_2 \leq y < -L_1 \text{ and } L_1 \leq y < L_2, \end{cases}$$

$$\phi(y, d) = 0.$$

$2L_1$ and $2(L_2 - L_1)$ are respectively the widths of the two regions of different alignments. d is the cell gap.

The one-constant approximation was used for LC elastic constants. The deformation free-energy density (f_d) was expressed as $f_d = \frac{K}{2} \{(\nabla \cdot \mathbf{n})^2 + (\nabla \times \mathbf{n})^2\}$. \mathbf{n} was the director and it was expressed as $(\cos \phi(y, z), \sin \phi(y, z), 0)$. K is the elastic constant. Under these conditions, $\phi(y, z)$ satisfies $\nabla^2 \phi = 0$. The solution satisfying the boundary conditions inside the cell is given by

$$\phi(y, z) = \frac{\pi}{2} \left(\frac{d-z}{d} \right) \left(\frac{L_1}{L_2} \right) + \sum_{m=1}^{\infty} \frac{1}{m} \sin \left(\frac{L_1}{L_2} m \pi \right) \times \cos \left(\frac{m \pi}{L_2} y \right) \frac{\sinh \left(\frac{m \pi}{L_2} (d-z) \right)}{\sinh \left(\frac{m \pi}{L_2} d \right)}. \quad (1)$$

Figure 1(b) shows the texture of the twist and parallel alignment regions, with the brightness change matching the angle variation in the above equation. In the texture, particles with a homeotropic alignment exhibit a hedgehog defect or Saturn-ring disclination, as shown in Figs. 1(c) and 1(d). Figure 1(c) presents a DC particle with a hyperbolic hedgehog defect, and Fig. 1(d) displays a QC particle with a Saturn-ring defect. The line connecting the defect and particle centers is inclined to the diagonal. It indicates that the particles are not

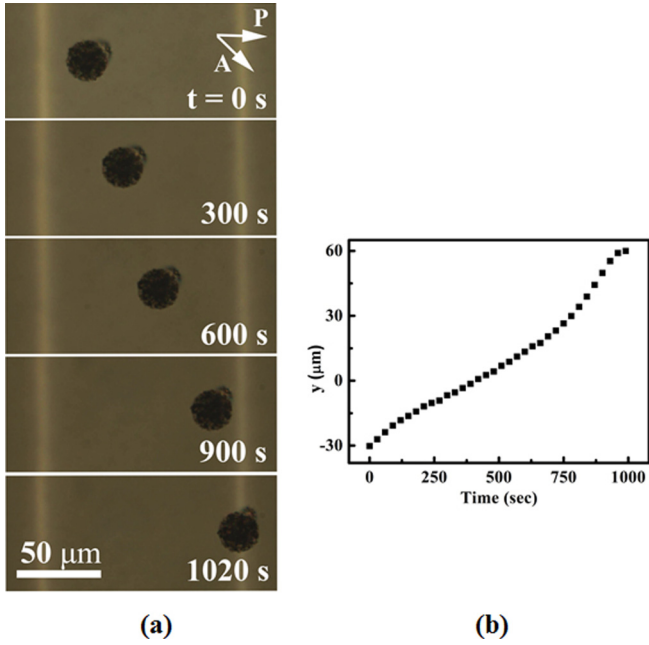


FIG. 2. (a) Images of a DC particle moving along the y direction acquired at different time intervals. (b) Graph of the particle position as a function of time. The position at $y = 0$ corresponds to the center of the twist region, and that at time $t = 0$ s corresponds to the onset of observation. The bright lines in (a) represent the boundary between the twist and parallel alignment regions. The radius of the particle equals $11.9 \mu\text{m}$.

close to the upper or lower substrates, but rather located near the middle of the cell along the z axis.

DC particles moved in the positive y direction, heading toward the hyperbolic hedgehog defect [Fig. 2(a)]. Movement in the x direction was not observed for the director field invariant along the x axis. When the hyperbolic hedgehog defect was located at the opposite side, the particles moved in the opposite direction, heading toward the defect. Generally, this movement did not occur at a constant speed [Fig. 2(b)], being relatively fast close to the boundary and relatively slow in the middle of the alignment region. At the boundary, the particle abruptly stopped. The corresponding position versus time graph shows a weak S-shaped motion.

In contrast to DC particles, QC particles exhibited little position changes in the twist and parallel alignment regions (Fig. 3). In Fig. 3(a), the QC particle stayed still in almost the same position. Figure 3(b) presents several examples of QC particle movement. Particles were stable at the initial position or moved to the right or left side by a small distance, except for “2” and “3.” This tiny positional variation of QC particles may be induced by interactions with deformations, the minute flow of LCs in the cell, or other factors. Particles with extraordinary motion such as “2” and “3” indicated a distorted Saturn ring with broken symmetry as in the small particle images in Fig. 3(b). Importantly, the QC particle movement is negligible compared to that of DC particles and is irreducible to rule.

In a planar aligned cell, the interaction between homeotropically aligned particles at the surface is analogous to that between electric point dipoles or quadrupoles [7]. We introduced dipole and quadrupole moment densities for the calculation of

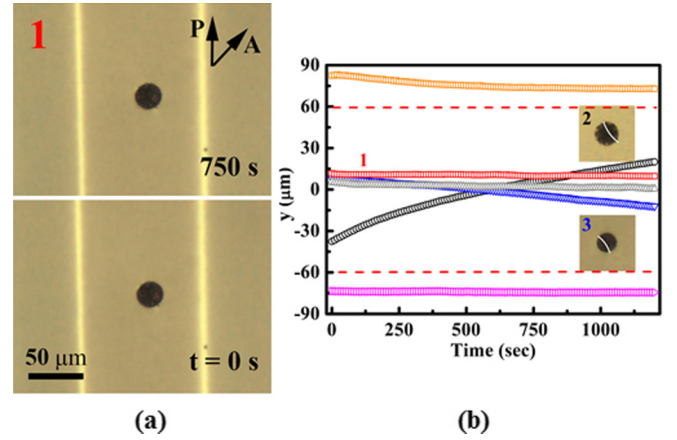


FIG. 3. Positional variation of a QC particle as a function of time. (a) Images of a QC particle for different times. (b) Experimental results showing the positional variation of different particles (indicated by different symbols and colors). “1” indicates the particles in (a). “2” and “3” images show the distorted QC particles. The white lines in two small particle images guide the Saturn ring of each particle. The others have clean QC with an expected symmetric Saturn-ring. $y = 0$ corresponds to the center of the twist region.

the interaction energies in NLCs. The magnitudes of the dipole and quadrupole moment densities of a particle with infinite anchoring are $P = \alpha R^2 \delta(\vec{r})$ and $C = \beta R^3 \delta(\vec{r})$, respectively, where $\alpha = 2.04$, $\beta = 0.72$, and R is the radius of the particle [7]. In the above expression, both dipoles and quadrupoles were assumed to be points at the origin.

The dipole orientation was considered to match the average director orientation around the particle. Among the two freedoms of \mathbf{n} , the dipole direction was defined as the orientation from the defect to the center of the particle. The particles used in this experiment did not exhibit strong anchoring, and neither α nor β is exactly known because of the unknown real distribution of the director field. We present effective dipole and quadrupole moment densities as $P_{\text{eff}} = \alpha \zeta^2 R^2 \delta(\vec{r})$ and $C_{\text{eff}} = \beta \zeta^3 R^3 \delta(\vec{r})$. The coefficient ζ can be related to the anchoring strength [8], or virtual radius for the effectiveness of the particles [28,29]. The values of ζ used were 0.73 for the DC particles and 0.62 for the QC particles in the calculation [28,29].

As the director field in the cell was not uniform, the dipole and quadrupole moments were not constant, varying with position in the y and z directions. However, we assumed that the dipole and quadrupole moments are ideal points, independent of the changing position.

The interaction energy between the dipole and director field is expressed as follows [7],

$$\mathcal{F}_P = 4\pi K \int d\tau [-\mathbf{P}_{\text{eff}} \cdot \mathbf{n}(\nabla \cdot \mathbf{n}) + \beta \mathbf{P}_{\text{eff}} \cdot (\mathbf{n} \times \nabla \times \mathbf{n})], \quad (2)$$

where β is a material-independent dimensionless parameter. We assume $\mathbf{P}_{\text{eff}} = P_{\text{eff}} \mathbf{n}$. The actual direction of \mathbf{P}_{eff} is decided by the relative positions between the point defect and the particle. It leads to $\mathcal{F}_P = -4\pi K P_{\text{eff}} (\nabla \cdot \mathbf{n})$ and subsequently to $\mathcal{F}_P = -4\pi K P_{\text{eff}} \cos \phi \partial \phi / \partial y$ for

$\mathbf{n} = (\cos \phi(y, z), \sin \phi(y, z), 0)$. From the above free energy, the force acting on the particle is given by

$$\begin{aligned} \vec{F}_P &= -\nabla \mathcal{F}_P \\ &= 4\pi K P_{\text{eff}} \left(0, \left(-\sin \phi \left(\frac{\partial \phi}{\partial y} \right)^2 + \cos \phi \frac{\partial^2 \phi}{\partial y^2} \right), \right. \\ &\quad \left. \left(-\sin \phi \frac{\partial \phi}{\partial y} \frac{\partial \phi}{\partial z} + \cos \phi \frac{\partial^2 \phi}{\partial z \partial y} \right) \right). \end{aligned} \quad (3)$$

Similarly, the interaction energy between the QC particle and the director field is expressed as [7]:

$$\begin{aligned} \mathcal{F}_C &= 4\pi K \int d\tau [(\nabla \cdot \mathbf{n})\mathbf{n} \cdot \nabla(n_i C_{ij} n_j) \\ &\quad + \nabla(n_i C_{ij} n_j) \cdot (\mathbf{n} \times \nabla \times \mathbf{n})], \end{aligned} \quad (4)$$

where C_{ij} is the quadrupole moment density. Since $n_i C_{ij} n_j$ can be expressed as $C\delta(\vec{r})$, we can write the interaction energy as

$$\mathcal{F}_C = -4\pi K C [\mathbf{n} \cdot \nabla(\nabla \cdot \mathbf{n}) + (\nabla \cdot \mathbf{n})^2 + \nabla \cdot (\mathbf{n} \times \nabla \times \mathbf{n})]. \quad (5)$$

For $\mathbf{n} = (\cos \phi(y, z), \sin \phi(y, z), 0)$, \mathcal{F}_C becomes zero. Since the above approximation tends to zero, the energy excited due to the inclusion of the QC particle is considered negligible, and this is in agreement with the theoretical prediction [14,15]. Figure 3 shows that the obtained results match this estimate.

Figure 4(a) shows the free energy of interaction of the DC particle for different positions inside the cell. In this calculation, the director was computed using experimental cell conditions of the width of the twist region ($2L_1 = 120 \mu\text{m}$), the width of the parallel region [$2(L_2 - L_1) = 80 \mu\text{m}$], and the cell gap ($70 \mu\text{m}$). The DC particle exhibited a high free energy of interaction at $y = -L_1$ [left boundary in Fig. 2(a)] and a low interaction energy at $y = L_1$ [right boundary in Fig. 2(a)].

For a particle inside the cell, we expected a right-hand movement to minimize the free energy. Moreover, since the interaction energy changes in the z direction, we also expected a movement in this direction. The force [$\vec{F}_P(y, z)$] acting on a DC particle is shown in Fig. 4(b). Importantly, we see that a y -directional force is present throughout the cell. The z -directional force changes direction at the left and right boundaries. The particle experiences a force in the positive z direction at the left boundary that is reversed to the negative z direction at the right boundary. Overall, the force is strong near the boundary and weak in the middle of the twist region. In the parallel alignment region, the y -directional force acting on the particle is reversed. Thus, to the right of the right boundary (at $60 \mu\text{m}$) on the y axis (parallel alignment region), the particle is pushed to the left, while to the left of the left boundary (at $-60 \mu\text{m}$) on the y axis (parallel alignment region), it is pushed to the right.

The reason behind the particle movement is the splay deformation of the director field. Since the edge of the DC particle hedgehog defect exhibits heavy splay deformation, the particle is attracted or repelled according to the dipole orientation, in good agreement with the experimental results.

Let us consider the movement of a DC particle inside the cell. Figures 4(a) and 4(b) indicate that besides the y

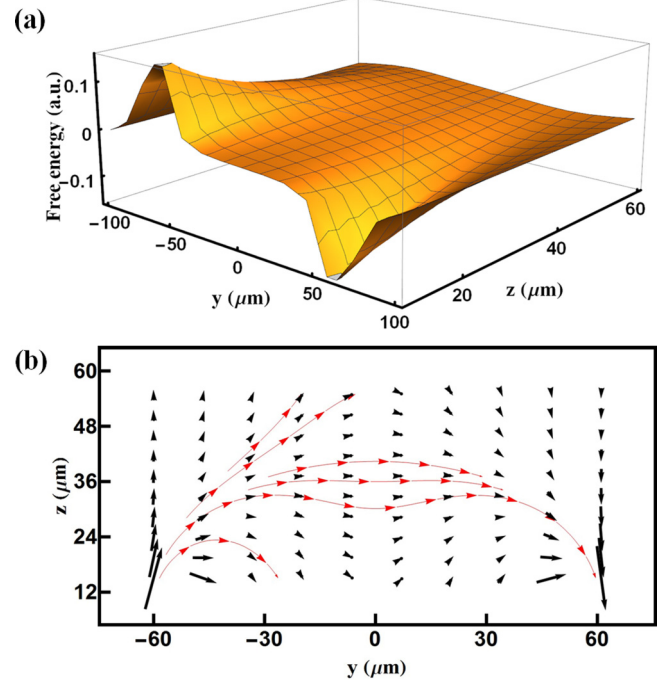


FIG. 4. (a) Free energy of interaction (\mathcal{F}_P) calculated for a DC particle in different positions in the twist region. The dipole of the DC particle is assumed to be oriented along the $-y$ direction, in line with the experimental result shown in Fig. 2. (b) Force $\vec{F}_P(y, z)$ acting on the DC particle in the twist region. The black arrows indicate the strength and direction of the force. Red solid arrow lines represent the possible paths of a particle in a quasiequilibrium state for different initial positions.

position, the z position is also important for determining the particle trajectory. Four forces act in the z direction, i.e., \vec{F}_P , interactions (\vec{F}_{mirror}) of the particle with upper/lower substrates, buoyancy ($\vec{F}_{\text{buoyancy}}$) due to the LC/particle density difference, and the Stokes drag force (\vec{F}_{Stokes}) hindering particle movement. In contrast, the forces acting in the y direction are \vec{F}_P and the Stokes drag force.

The substrate-particle interaction force is given by $\vec{F}_{\text{mirror}} = 36\pi K P^2 \left(\frac{1}{(2z)^4} - \frac{1}{\{2(d-z)\}^4} \right) \hat{z}$ [14,17]. This originated from the boundary condition on the substrate [14,15]. Both upper and lower substrates induce the repulsive force to the particle. The first term represents the contribution of the upper substrate, and the second term corresponds to that of the lower one. Since the above equation was obtained assuming uniform alignment, care should be taken in applying it to the twist structure ($y \sim 0$) or near the boundary ($y = -L_1$ or L_1) between the twist and parallel regions.

The buoyancy due to the different densities of the LC and the particle is expressed as $\vec{F}_{\text{buoyancy}} = -\frac{4}{3}\pi R^3(\rho_{\text{LC}} - \rho_{\text{particle}})g\hat{z}$, where ρ_{LC} and ρ_{particle} are the respective densities, and g is the gravitational acceleration.

The Stokes drag force acts on the moving particle and it is opposite to the direction of movement. For movement in the y direction, the drag force is given by $\vec{F}_{\text{Stokes}}^y = -6\pi R\gamma_y v_y \hat{y}$, whereas for z -directional movement, the force equals $\vec{F}_{\text{Stokes}}^z = -6\pi R\gamma_z v_z \hat{z}$. Here, γ_y and γ_z are the effective viscosities of

the LC in the direction of movement that we assumed to equal $3.1 \times 10^{-3} \text{ N s/m}^2$ in the calculation. v_y and v_z are the velocities in the y and z directions, respectively.

The total force (\vec{F}) is obtained by adding all the above-mentioned forces. As the velocity change is small, motion occurs without acceleration, and the force can be approximated as $\vec{F} = 0$:

$$\vec{F} = \vec{F}_P + \vec{F}_{\text{mirror}} + \vec{F}_{\text{buoyancy}} + \vec{F}_{\text{Stokes}}. \quad (6)$$

The forces act in the y and z directions with \vec{F}_{mirror} and $\vec{F}_{\text{buoyancy}}$ acting in the z direction only.

Under these conditions,

$$F_y = \hat{y} \cdot [\vec{F}_P + \vec{F}_{\text{Stokes}}] \sim 0, \quad (7)$$

$$F_z = \hat{z} \cdot [\vec{F}_P + \vec{F}_{\text{mirror}} + \vec{F}_{\text{buoyancy}} + \vec{F}_{\text{Stokes}}] \sim 0. \quad (8)$$

Since these equations are difficult to solve analytically, we solved them using numerical calculations. We obtain particle trajectories with initial positions on the y and z axes.

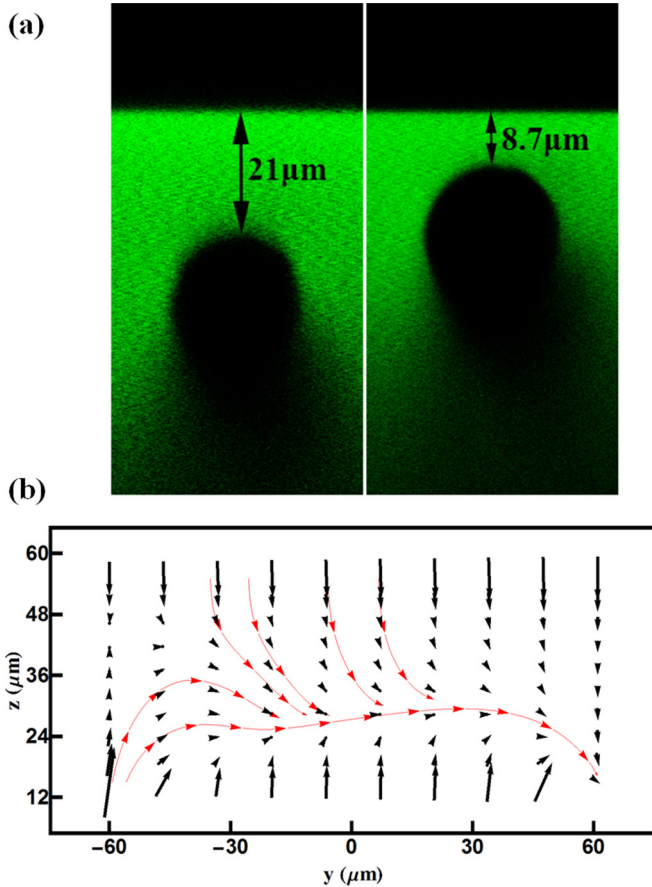


FIG. 5. (a) Side views of a particle in the LC cell obtained with a confocal microscope. The left image corresponds to the middle of the twist region, while the right image was acquired near the boundary. The z position of the particle is the farthest from the upper substrate in the middle of the twist region, getting closer upon approaching the boundary. (b) Force acting on the particle (black arrows) and trajectories of particles (red arrow lines) starting from different positions inside the LC cell.

The dependence of the particle height on its position in the LC cell is shown in Fig. 5(a). The z position of the particle is the farthest from the upper (patterned) substrate in the middle of the twist region, getting close upon approaching the boundary. This result means that height variations should be considered for tracking particle movement. Figure 5(b) presents the result obtained by considering both the y and z directions in the force calculation. The particle motion was assumed to occur close to the equilibrium position at a very slow speed [Fig. 5(b)]. Moreover, the interaction of the particle near the boundary with upper and lower substrates may not be identical to that observed at the center of the twist region; however, this variation was neglected. The particle experiences an increasing force in the z direction at the left boundary, which is reversed at the right boundary. Due to the interaction with the upper and lower substrates, the particle is not absorbed by the substrates. The calculated trajectories for different initial positions are shown by the red lines in Fig. 5(b), with different initial positions resulting in different trajectories. However, a quasistable trajectory seems to exist, and the particles try to follow it despite the different initial positions. Thus, we expect most of the trajectories to be similar to the quasistable trajectory [32].

Figure 6 shows several particle trajectories in the y direction and the fitted result obtained by adjusting the initial conditions. Different initial positions result in a little different trajectory to reach to the boundary (corresponding to $60 \mu\text{m}$ on the y axis) between the twist and parallel alignment regions. Despite the small differences, all trajectories follow similarly shaped paths, with rather slow movement near the middle of the twist region and fast movement near the boundary. All fitted results are in good agreement with the experimental data obtained at a large distance from the boundary, slightly deviating from the experimental values near the boundary. This may be due to the violation of the assumptions made in the calculation, such as the point dipole character of the particles, the uncertainty of the interaction with the substrates near the boundary, and the change in the involved material parameters near the boundary.

The trajectories were calculated using Eqs. (7) and (8). Several parameters, such as the elastic constant (K), viscosity, particle radius, ζ , and α , were involved in the calculation. These parameters were grouped into two terms,

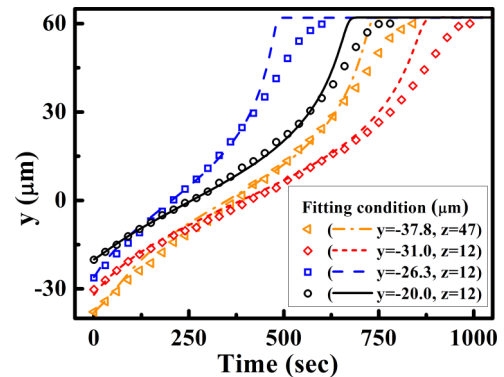


FIG. 6. Experimental and calculated particle trajectories. Different experimental trajectories were fitted by adjusting the initial conditions. Time $t = 0 \text{ s}$ corresponds to the onset of observation.

$A = (4\pi K\alpha\zeta^2 R^2)$ and $B = (6\pi\gamma R)$, which were adjusted within $\pm 20\%$ of the values reported in literature to find an appropriate initial position in the z direction. The uncertainty in the values of all the physical parameters justifies this approach. The initial y position was obtained based on the texture image, and the z position was obtained based on the best-fit result. The different initial positions originated from heating the cell above the isotropic phase transition temperature and cooling it down. The LC phase transition forced the particles to move away from their original positions, resetting the movement to start at another initial position. In the case of different particles, their different sizes and anchoring strengths changed their effective interactions.

IV. CONCLUSIONS

We demonstrate the peculiar behavior of a single particle in a deformed NLC director field. In this experiment, an alignment pattern was constructed for the deformed director structure. The particle moves to the most energetically stable position. Splay deformation pushes dipole-configuration par-

ticles to the position of heavy splay heading the point defect in the twisted region. In contrast, the quadrupole particles seem to be stabilized in any location due to the small free-energy differences between the different positions. The model calculation is in good agreement with experimental observations. The results indicate that it is possible to intentionally control colloid particles with a designed alignment and construct the desired particle structure in NLC cells.

ACKNOWLEDGMENTS

This research was supported by the Basic Science Research Program through the National Research Foundation of Korea (NRF) funded by the Ministry of Education, Science and Technology (NRF-2014R1A1A2058029), and supported by the Brain Pool Program through the Korean Federation of Science and Technology Societies (KOFST) funded by the Ministry of Science, ICT and Future Planning (161S-1-3-1617).

B.K.L. and S.J.K. contributed equally to this work.

-
- [1] P. G. de Gennes and J. Prost, *The Physics of Liquid Crystals* (Oxford University Press, New York, 1993).
- [2] E. M. Terentjev, *Phys. Rev. E* **51**, 1330 (1995).
- [3] O. V. Kuxsenok, R. W. Ruhwandl, S. V. Shiyakovskii, and E. M. Terentjev, *Phys. Rev. E* **54**, 5198 (1996).
- [4] P. Poulin, V. Cabuil, and D. A. Weitz, *Phys. Rev. Lett.* **79**, 4862 (1997).
- [5] P. Poulin, H. Stark, T. C. Lubensky, and D. A. Weitz, *Science* **275**, 1770 (1997).
- [6] P. Poulin and D. A. Weitz, *Phys. Rev. E* **57**, 626 (1998).
- [7] T. C. Lubensky, D. Petey, N. Currier, and H. Stark, *Phys. Rev. E* **57**, 610 (1998).
- [8] B. I. Lev and P. M. Tomchuk, *Phys. Rev. E* **59**, 591 (1999).
- [9] R. W. Ruhwandl and E. M. Terentjev, *Phys. Rev. E* **54**, 5204 (1996).
- [10] R. W. Ruhwandl and E. M. Terentjev, *Phys. Rev. E* **56**, 5561 (1997).
- [11] O. D. Lavrentovich, I. Lazo, and O. P. Pishnyak, *Nature (London)* **467**, 947 (2010).
- [12] S. Chono and T. Tsuji, *Mol. Cryst. Liq. Cryst.* **309**, 217 (1998).
- [13] N. Kondo, Y. Iwashita, and Y. Kimura, *Phys. Rev. E* **82**, 020701 (2010).
- [14] T. Kishita, N. Kondo, K. Takahashi, M. Ichikawa, J. I. Fukuda, and Y. Kimura, *Phys. Rev. E* **84**, 021704 (2011).
- [15] S. B. Chernyshuk and B. I. Lev, *Phys. Rev. E* **84**, 011707 (2011).
- [16] S. B. Chernyshuk and B. I. Lev, *Phys. Rev. E* **81**, 041701 (2010).
- [17] J. Fukuda, B. I. Lev, and H. Yokoyama, *J. Phys.: Condens. Matter* **15**, 3841 (2003).
- [18] J. I. Fukuda, B. I. Lev, and H. Yokoyama, *Phys. Rev. E* **65**, 031710 (2002).
- [19] S. B. Chernyshuk, O. M. Tovkach, and B. I. Lev, *Phys. Rev. E* **85**, 011706 (2012).
- [20] J. I. Fukuda, B. I. Lev, K. M. Aoki, and H. Yokoyama, *Phys. Rev. E* **66**, 051711 (2002).
- [21] E. B. Kim, O. Guzman, S. Grollau, N. L. Abbott, and J. J. de Pablo, *J. Chem. Phys.* **121**, 1949 (2004).
- [22] M. Yada, J. Yamamoto, and H. Yokoyama, *Phys. Rev. Lett.* **92**, 185501 (2004).
- [23] P. C. Mushenheim, R. R. Trivedi, H. H. Tuson, D. B. Weibel, and N. L. Abbot, *Soft Matter* **10**, 88 (2014).
- [24] I. I. Smalyukh, J. Butler, J. D. ShROUT, M. R. Parsek, and G. C. L. Wong, *Phys. Rev. E* **78**, 030701(R) (2008).
- [25] M. Vilfan, N. Osterman, M. Copic, M. Ravnik, S. Zumer, J. Kotar, D. Babic, and I. Poberaj, *Phys. Rev. Lett.* **101**, 237801 (2008).
- [26] B. Park, Y. Jung, H. H. Choi, H. K. Hwang, Y. Kim, S. Lee, S. H. Jang, M. Kakimoto, and H. Takezoe, *Jpn. J. Appl. Phys.* **37**, 5663 (1998).
- [27] G. A. Oweimreen, A. K. Shihab, K. Halhouli, and S. F. Sikander, *Mol. Cryst. Liq. Cryst.* **138**, 327 (1986).
- [28] S. J. Kim and J. H. Kim, *Soft Matter* **10**, 2664 (2014).
- [29] S. J. Kim, B. K. Lee, and J. H. Kim, *Liq. Cryst.* **43**, 1589 (2016).
- [30] M. Cul and J. R. Kelly, *Mol. Cryst. Liq. Cryst.* **331**, 49 (1999).
- [31] H. Knepppe, F. Schneider, and N. K. Sharma, *Ber. Bunsenges. Phys. Chem.* **85**, 784 (1981).
- [32] B. Senyuk, M. C. M. Varney, J. A. Lopez, S. Wang, N. Wu, and I. I. Smalyukh, *Soft Matter* **10**, 6014 (2014).